PHYSICAL REVIEW B **81**, 125434 (2010)

Unusual Raman dispersion for *D* and 2*D* lines in high-curvature single-walled carbon nanotubes revealed by ^{13}C isotope substitution

F. Simon,[1,*] V. Zólyomi,[2,3] R. Pfeiffer,[1] H. Kuzmany,[1] J. Koltai,[4] and J. Kürti[4]
[1]*Faculty of Physics, University of Vienna, Strudlhofgasse 4, A-1090 Vienna, Austria*
[2]*Department of Physics, Lancaster University, Lancaster LA1 4YB, United Kingdom*
[3]*Research Institute for Solid State Physics and Optics, Hungarian Academy of Sciences, P.O. Box 49, H-1525 Budapest, Hungary*
[4]*Department of Biological Physics, Eötvös University, Pázmány Péter sétány 1/A, H-1117 Budapest, Hungary*
(Received 22 January 2010; published 26 March 2010)

The defect-induced *D* line and its overtone are fundamental signatures in the Raman spectra of carbon nanomaterials. An analysis of these lines as a function of laser excitation energy is reported for double-walled carbon nanotubes where the inner tubes represent high-curvature nanotube species. From ^{13}C substituted inner tubes it is demonstrated that the quasilinear relations between laser energy and line position (Raman dispersion) cross over unexpectedly for low-energy excitation for the inner and outer tube shells. The result is quantitatively explained by a curvature-induced phonon softening and first-principles calculations of the optical transition energies.

DOI: 10.1103/PhysRevB.81.125434 PACS number(s): 78.67.Ch, 63.20.D−, 78.30.Na, 78.66.Tr

I. INTRODUCTION

Carbon allotropes with different dimensionality[1,2] are in the focus of interest due to their compelling fundamental properties and application potential. Raman spectroscopy is a key analytical tool due to its large scattering cross section and the wealth of information it provides. The Raman response of the different allotropes such as fullerenes,[3] graphene,[4] single-walled carbon nanotubes (SWCNTs),[5] graphite, and diamond share many common features. Among the various vibrational modes, the defect-induced *D* mode around 1350 cm^{-1} and its overtone, the 2*D* (also known as D^* or G') mode around 2700 cm^{-1} are observed in sp^2 carbon materials.[6–9] The *D* and 2*D* modes are unique as their Raman shifts change linearly with the exciting laser energy by about 50 cm^{-1}/eV and 100 cm^{-1}/eV, respectively. This phenomenon is called *Raman dispersion*[10] since a change in the laser energy corresponds to a change in k vector in the scattering process. The *D* line is also widely used to characterize defect structure and grain size in carbonaceous materials.[11]

The *D* and 2*D* mode Raman dispersions were explained in graphite by a double resonance process which includes a scattering of the excited electron by a zone boundary phonon.[12] This distinguishes these modes from usual zone-center phonons. Thus, the study of *D* and 2*D* modes allows for a unique insight into the electronic and vibrational properties.[13] The double resonance model was extended to SWCNTs by considering the latter as curved graphene and by taking the additional effect of the Van Hove singularities into account.[14] It is generally accepted that SWCNTs with diameters above 1.3–1.4 nm do behave as curved graphene, however SWCNTs with diameters below 1 nm show non-graphene derived behavior and their curvature plays an important role. This leads to compelling phenomena, e.g., to superconductivity in zeolite-grown highly curved carbon nanotubes.[15]

Inner tubes of double-walled carbon nanotubes (DWCNTs) grown from C_{60} molecules encapsulated inside SWCNTs are ideal small diameter tubes which provide a test bed to study curvature-dependent effects. An additional benefit of the inner tubes is that they can be grown as ^{13}C enriched species (using isotope enriched fullerenes) while the outer tubes remain of natural carbon.[16] A downshift of the inner tube *D* and 2*D* modes was reported but the Raman dispersion itself was found independent[17] or only weakly dependent on tube diameter.[18,19] From these results in the visible spectral range, a crossover between the Raman dispersion of the outer and inner tubes is not expected.

Here, we report the anomalous Raman dispersion of the *D* and 2*D* modes for inner tubes with diameters as small as $d \approx 0.7$ nm. The respective modes from the inner tubes have smaller Raman shift for visible laser excitations (1.83–2.54 eV) but in contrast to expectations, the linear Raman dispersion from the outer and inner tubes cross for infrared excitation (1.16 eV). This result is confirmed from DWCNTs whose inner shell is ^{13}C enriched. First-principles calculations show a curvature-induced phonon softening. Including this softening in a parameterized phonon dispersion, together with considering curvature related changes in the electronic structure, explains the data.

II. EXPERIMENTAL

We studied DWCNT samples with inner walls of natural and 82% ^{13}C enriched carbon, denoted as ^{12}C and ^{13}C DWCNT, respectively. The diameter distributions of the outer and inner tubes were determined by a multilaser Raman measurement of the radial breathing mode following Ref. 20, which gave mean diameters of 1.4 nm and 0.7 nm, respectively. We also found that the inner and outer tube diameter distributions follow each other with the same, 0.1 nm, Gaussian variance of the diameter distributions. Raman spectroscopy was performed for the visible range (1.83–2.54 eV) and with an infrared excitation (1.16 eV). Phonon and electron dispersions were calculated at the first-principles level using density-functional theory (DFT) with the Vienna

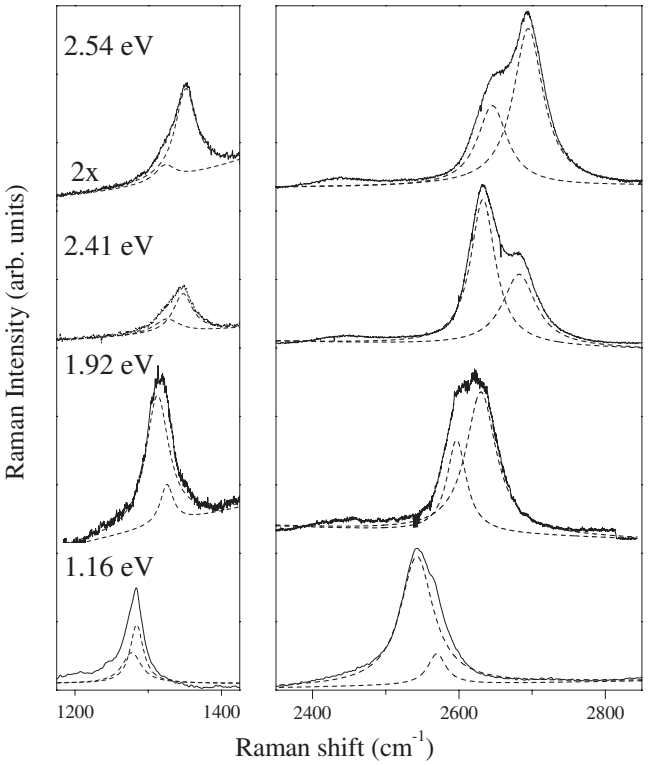

FIG. 1. Raman spectra of the *D* and 2*D* modes of ^{12}C DWCNTs for different excitations. Dashed curves are decompositions into two components.

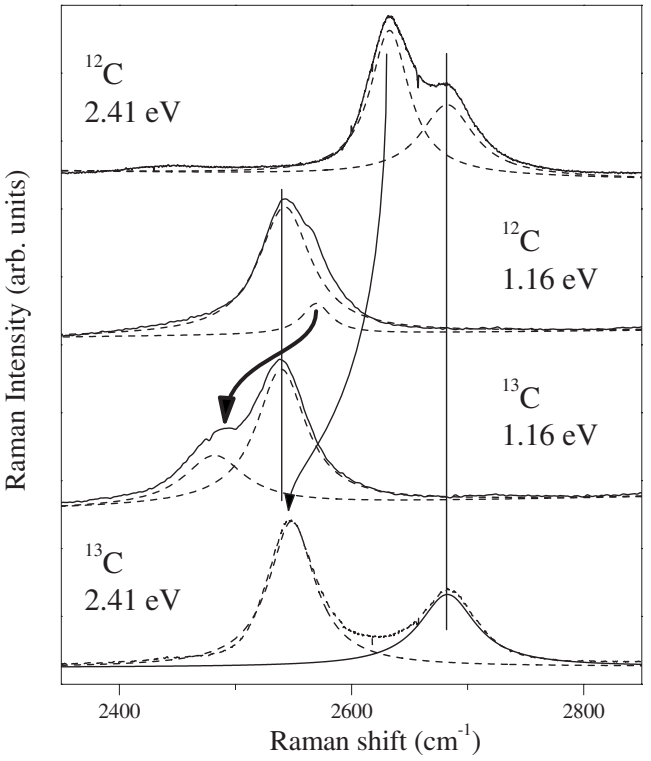

FIG. 2. The 2*D* Raman mode in ^{12}C (upper two spectra) and ^{13}C DWCNTs (lower two spectra) with 2.41 and 1.16 eV excitations. Curly arrows and vertical solid lines indicate the shifting inner-outer and the nonshifting outer tube modes, respectively. Thick arrow shows the anomalously shifting component.

ab initio simulation package [VASP (Ref. 21)] within the local-density approximation. A plane-wave basis set was used with a cutoff energy of 400 eV. Geometries were fully relaxed and the phonon dispersions were calculated from the dynamical matrix which was obtained by numerical differentiation of analytical Hellman-Feynman forces. Phonon dispersions are depicted in the so-called helical Brillouin zone (BZ), exploiting the helical symmetry of the nanotubes.[22] This is an extended zone picture for the SWCNTs with two carbon atom unit cells.[23]

III. RESULTS AND DISCUSSION

Figure 1 depicts the Raman spectra of the *D* and the 2*D* modes in ^{12}C DWCNTs excited with various lasers. Both modes can be fitted by two Voigtian curves (dashed curves in the figure). It was shown[19] for visible excitations (1.83–2.54 eV) that the two components of the 2*D* mode with higher and lower Raman shifts represent the response from the outer and inner tubes, respectively. The decomposition is less clear for the *D* mode but the inner and outer tube modes were identified previously with the help of ^{13}C labeling of inner tubes.[16]

One expects that the two components can be assigned similarly for the infrared excitation (1.16 eV). This is not the case. Rather, in this spectrum the component with larger Raman shift comes from *inner* tubes and the one with smaller Raman shift comes from *outer* tubes. This is clearly shown with the help of ^{13}C enriched inner tubes in Fig. 2. The 2*D* component that has a *larger* Raman shift is downshifted upon the isotope enrichment of the inner tubes for the 1.16 eV excitation. This contrast to visible excitations (e.g., 2.41 eV) where the component with the smaller Raman shift is downshifted upon isotope enrichment. The same is observed for the *D* mode (not shown) but we focus on the 2*D* mode in the following as therein Raman shift differences are twice as large. The magnitude of the downshift for the 2*D* mode is 85 cm^{-1}, which agrees with the value for visible excitations and also with that calculated from the mass enhancement of inner tubes. Peak positions, isotope downshifts, linearized Raman dispersion slopes, and mean deviation (σ) of the Raman dispersion from linearity for the 2*D* mode are given in Table I.

Figure 3 shows the 2*D* mode Raman shifts for the outer and inner tubes for a large number of excitation energies. In agreement with a previous report,[19] a reasonable linear Raman dispersion is observed for the outer tubes with a weak oscillatory behavior on top of it. It can be fitted with a straight line (upper solid curve in Fig. 3) $\omega(2D)=A+B*E_{\text{laser}}$ with a mean deviation σ of only 2.5 cm^{-1} and A and B of 2421 cm^{-1} and 108 cm^{-1}/eV, respectively.[24] A linear fit to the calculated Raman shifts, which is detailed below, reproduces the experimental data well (upper dashed curve in Fig. 3) with a Raman dispersion slope and σ of 106 cm^{-1}/eV and 3.8 cm^{-1}, respectively.

In contrast, Raman dispersion of the inner tube mode for both the ^{12}C and the ^{13}C samples (data not shown) is less

TABLE I. 2*D* Raman shifts, isotope downshifts, linearized Raman dispersion slopes (in cm^{-1}/eV units), and mean deviation from linearity, σ (in cm^{-1} units). Errors are ± 1 (Raman shifts) and ± 2 cm^{-1} (downshifts).

	^{12}C Inner/outer	^{13}C Inner/outer	Isotope shift Expt./calc.
2.41 eV	2632/2682	2549/2682	83/84
1.16 eV	2570/2542	2481/2540	89/82
Disp. slope (σ), expt.	62(5.9)/108(2.5)		
Disp. slope (σ), calc.	64(7.3)/106(3.8)		

linear with a larger slope at higher energy excitations than at low energies. When fitted by a linear function, the inner tube data yields A and B of 2486 cm^{-1} and 62 cm^{-1}/eV, and $\sigma = 5.9$ cm^{-1}. The latter is more than a factor two larger than the corresponding value for the outer tubes. Again, the experimental data are well reproduced by a linear fit (lower dashed curve in Fig. 3) to the calculated 2*D* Raman shifts (details are given below) with a Raman dispersion slope of 64 cm^{-1}/eV and $\sigma = 7.3$ cm^{-1}.

In the following, we explain the observed 2*D* Raman mode softening and the anomalous Raman dispersion for the small diameter tubes. The double resonance theory for graphite[12] considers scattering between the two inequivalent **K** points of the graphene BZ. For SWCNTs, resonance between the Van Hove singularities and the exciting laser is of importance (the so-called triple resonance).[14] In the single particle description, the optical transition energy equals the energy difference between Van Hove singularities.

Clearly, knowledge of the curvature-dependent phonon and electron dispersions is required to account for the data. Figure 4 shows a first-principles result of the phonon dispersion for the (7,3) and (14,6) SWCNTs. These tubes have diameters of 0.699 nm and 1.388 nm, respectively, which make them representative for an inner-outer tube pair in our samples. We observe a softening in the phonon energy of up to 60 cm^{-1} for the smaller inner tube and a strong dependence of this softening on the k vector. Similar results were obtained for a number of other relevant pairs of tubes.

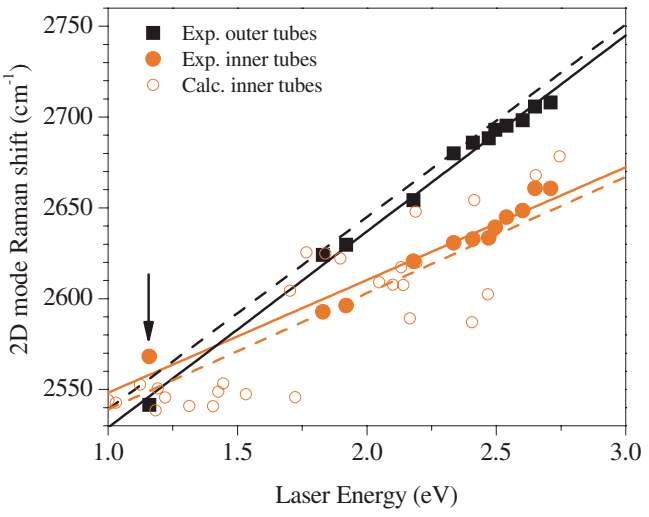

FIG. 3. (Color online) The 2*D* mode Raman dispersion for the outer and inner tubes of ^{12}C-DWCNT samples. Arrow highlights the anomalous inner tube 2*D* mode at 1.16 eV excitation. Calculated points correspond to individual tubes within the inner tube diameter distribution. Solid and dashed curves are linear fits to measured and calculated 2*D* Raman mode shifts (see text), respectively.

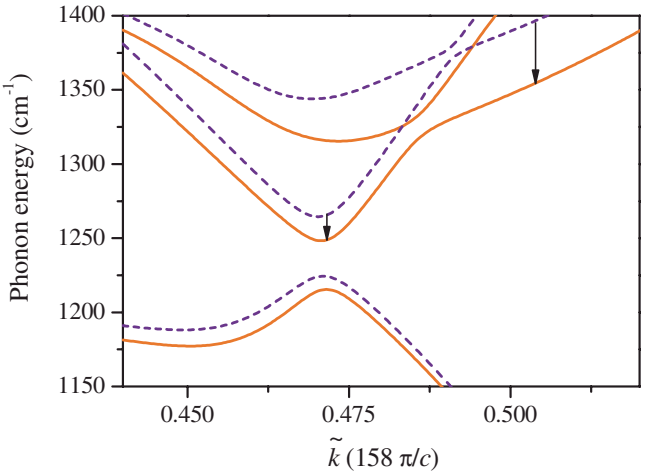

FIG. 4. (Color online) Phonon dispersion in the helical Brillouin zone around the **K** point in SWCNTs; solid curves: (7,3), dashed curves: (14,6). The BZ boundaries are at $158\pi/c$ $[-1,1]$ in units of the symmetry adapted wave number, $\tilde{k}$. Arrows indicate the $\tilde{k}$-dependent phonon softening for the smaller SWCNT.

In principle, DFT-based electron and phonon dispersions would yield a robust, first-principles result on the *D* and 2*D* Raman modes. However, this calculation cannot be performed for all relevant nanotubes. The DFT-based electron dispersion requires quasiparticle corrections and the phonon dispersion for metallic nanotubes is known to display Kohn anomalies.[25] The calculation of both of these effects is unfeasible at the DFT level for chiral nanotubes which constitute the majority (up to 80%) of a typical sample.[2] We therefore explain the experimental data using a parameterized phonon dispersion which however adopts the most important observation of the DFT result, the **k**-dependent phonon softening. We include the electron dispersion from a DFT calculation which is scaled to known experimental data[26,27] to provide accurate optical Van Hove transition energies. The parameters of the phonon dispersion are free and are adjusted to our measurement. It is described by,

$$\omega(k_r,k_\phi) = \{\omega_K + \omega_1 k_r[1 - \delta\cos(3k_\phi)]\}\left(1 - \frac{Ck_r^2}{d_t^2}\right). \quad (1)$$

Here, the k_r and k_ϕ are polar coordinates of the vector $\mathbf{k} - \mathbf{K}$, where **k** is determined by the Van Hove singularities (i.e., where a cutting line touches an energy contour[28]) as it is shown by an arrow in Fig. 5(a). for the (7,3) tube. ω_K, ω_1 are empirical parameters, $\delta = 0.06$ accounts for the so-called trigonal warping effect.[14] We found that the phonon softening can be well described by the softening factor, $1 - \frac{Ck_r^2}{d_t^2}$, which is quadratic in k_r and depends on the tube diameter, d_t.

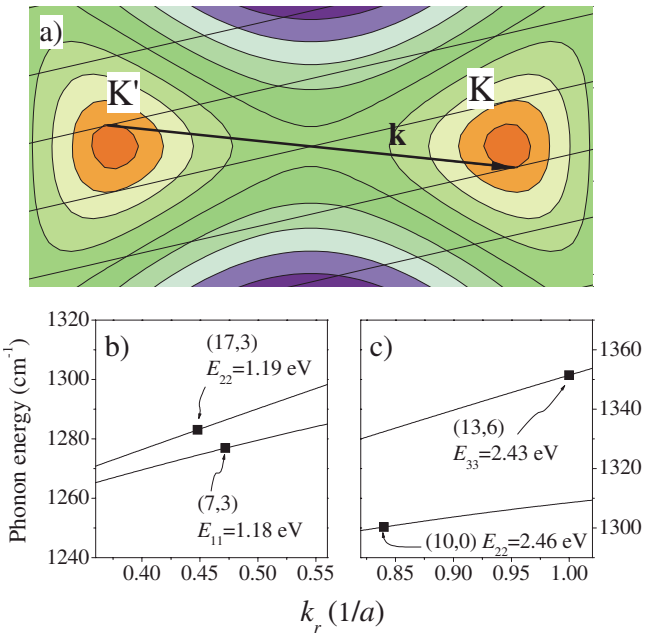

FIG. 5. (Color online) (a) Triple resonance scenario in the small diameter (7,3) tube and [(b) and (c)] the calculated phonon energy as a function of k_r for tubes which are in resonance around 1.2 and 2.5 eV. Symbols show the k_r values selected by the resonance condition for the given tubes. Note that k_r is larger for the (7,3) tube than for the (17,3), which partially compensates for the softening.

The 2*D* mode Raman shifts are calculated with this model phonon dispersion (open symbols in Fig. 3) as depicted in Fig. 5(a). The **k** vector is determined in the triple resonance approximation by the position of the Van Hove singularities: it connects the BZ points where the cutting line of the right transition branch touches an equienergy contour near the **K**′ and **K** points. The touching lines depend only on the (n,m) chiral indices of the SWCNTs, however, the components of **k** strongly depend on the electron energy dispersion. k_r and k_ϕ determine the phonon energy according to Eq. (1). which is half the Raman shift of the two-phonon 2*D* Raman mode.

A linear fit to the calculated 2*D* mode Raman shifts yields the linearized Raman dispersion for both the outer and inner tubes (dashed lines in Fig. 3). The best agreement between the experimental linearized Raman dispersions (solid lines in Fig. 3) and the calculated ones are obtained for $\omega_K = 1219$ cm^{-1}, $\omega_1 = 140$ cm^{-1} a, and $C = 0.0192$ nm^2 a^2, where a is the graphene lattice constant and k_r is measured in units of $1/a$.

This gives a Raman dispersion slope of $B = 64$ cm^{-1}/eV and $\sigma = 7.3$ cm^{-1} for the inner tubes. Clearly, the model yields a good quantitative agreement between the experiment and calculation in addition to describing the observed behavior qualitatively; i.e., (i) crossing of the inner and outer tube Raman dispersion lines, (ii) smaller Raman dispersion slope for the inner tubes, and (iii) larger mean deviation from linearity for the inner tubes than for the outer ones. The larger scattering seen for the inner tube 2*D* Raman modes, is an inherent property of the so-called family behavior, i.e., tubes with similar diameters can have very different optical transition energies.[29]

Finally, we give a qualitative explanation for the observed anomalous behavior. In general, the Raman dispersion slope of the *D* and 2*D* modes is related to the curvature (i.e., second derivative) of the phonon dispersion around the **K** point. As we observe in the DFT calculations, not only the absolute value but also the second derivative of the phonon dispersion decreases with decreasing tube diameter. This explains the smaller Raman dispersion slope for the inner tubes. However, this alone is not enough to explain the crossing of the Raman dispersion lines. It is a consequence of the electronic structure.

Figures 5(b) and 5(c) show phonon dispersions for two inner-outer tube pairs which have nearly equal optical transitions around 1.2 eV and 2.5 eV, respectively. Solid lines are calculated according to Eq. (1) as a function of k_r. The larger separation between the solid lines for larger k_r's is due to the k dependence of the softening. The k_r values for an inner and outer tube swap order for the two different excitation energies: k_r is larger for the outer tube at 2.5 eV, whereas it is larger for the *inner* tube at 1.2 eV. The softening of the inner tube phonon dispersion is therefore partially compensated by the larger k_r values, which causes the crossing of the Raman dispersion lines at small excitation energies. This behavior of the k_r is due to the fact that the electron energy dispersion is softened by the curvature in the vicinity of the **K** point for small diameter tubes. This is known as the *redshift* of the optical transition energies[26,27,30,31] and curvature-induced changes of this kind were first described in Ref. 32. It means that for a given laser excitation a *smaller* diameter inner tube is in resonance than expected without the redshift effect. A smaller diameter inner tube has necessarily sparser cutting lines, which gives rise to the larger k_r.

IV. CONCLUSIONS

In summary, we presented energy-dispersive Raman data for the *D* and 2*D* modes in DWCNTs. The Raman dispersion slope is smaller for inner than for outer tubes and at low-energy excitations the inner and outer tube Raman lines reverse their positions. First-principles calculations indicate a curvature-induced and wave-vector-dependent phonon energy softening. Including this effect in a model phonon dispersion, together with the curvature related redshift of the first optical transition in small diameter tubes allows to explain the data quantitatively.

ACKNOWLEDGMENTS

Supported by the FWF under Grant No. I83-N20, OTKA under Grants No. F68852, No. K60576, and No. NI67702, and the MCIEF-220094 projects and the Bolyai program of the Hungarian Academy of Sciences.

*Corresponding author. ferenc.simon@univie.ac.at

[1] M. Dresselhaus, G. Dresselhaus, and P. C. Ecklund, *Science of Fullerenes and Carbon Nanotubes* (Academic Press, New York, 1996).
[2] R. Saito, G. Dresselhaus, and M. Dresselhaus, *Physical Properties of Carbon Nanotubes* (Imperial College Press, London, 1998).
[3] H. W. Kroto, J. R. Heath, S. C. O'Brien, R. F. Curl, and R. E. Smalley, Nature (London) **318**, 162 (1985).
[4] K. S. Novoselov, A. K. Geim, S. V. Morozov, D. Jiang, Y. Zhang, S. V. Dubonos, I. V. Grigorieva, and A. A. Firsov, Science **306**, 666 (2004).
[5] S. Iijima and T. Ichihashi, Nature (London) **363**, 603 (1993).
[6] F. Tuinstra and J. L. Koenig, J. Chem. Phys. **53**, 1126 (1970).
[7] J. M. Holden Z. Ping, X. X. Bi, P. C. Eklund, S. J. Bandow, R. A. Jishi, K. Daschowdhury, G. Dresselhaus, and M. S. Dresselhaus, Chem. Phys. Lett. **220**, 186 (1994).
[8] A. C. Ferrari, J. C. Meyer, V. Scardaci, C. Casiraghi, M. Lazzeri, F. Mauri, S. Piscanec, D. Jiang, K. S. Novoselov, S. Roth, and A. K. Geim, Phys. Rev. Lett. **97**, 187401 (2006).
[9] L. Malard, D. Mafra, S. Doorn, and M. Pimenta, Solid State Commun. **149**, 1136 (2009).
[10] R. P. Vidano, D. B. Fischbach, L. J. Willis, and T. M. Loehr, Solid State Commun. **39**, 341 (1981).
[11] R. J. Nemanich and S. A. Solin, Phys. Rev. B **20**, 392 (1979).
[12] C. Thomsen and S. Reich, Phys. Rev. Lett. **85**, 5214 (2000).
[13] R. Saito, A. Jorio, A. G. Souza, A. Grueneis, M. A. Pimenta, G. Dresselhaus, and M. S. Dresselhaus, Physica B **323**, 100 (2002).
[14] J. Kürti, V. Zólyomi, A. Grüneis, and H. Kuzmany, Phys. Rev. B **65**, 165433 (2002).
[15] Z. K. Tang, L. Y. Zhang, N. Wang, X. X. Zhang, G. H. Wen, G. D. Li, J. N. Wang, C. T. Chan, and P. Sheng, Science **292**, 2462 (2001).
[16] F. Simon, C. Kramberger, R. Pfeiffer, H. Kuzmany, V. Zólyomi, J. Kürti, P. M. Singer, and H. Alloul, Phys. Rev. Lett. **95**, 017401 (2005).
[17] E. Barros *et al.*, Phys. Rev. B **76**, 045425 (2007).
[18] A. G. Souza-Filho, A. Joria, G. G. Samsonidze, G. Dresselhaus, M. A. Pimenta, M. S. Dresselhaus, A. K. Swan, M. S. Ünlü, B. B. Goldberg, and R. Saito, Phys. Rev. B **67**, 035427 (2003).
[19] R. Pfeiffer, H. Kuzmany, F. Simon, S. N. Bokova, and E. Obraztsova, Phys. Rev. B **71**, 155409 (2005).
[20] H. Kuzmany, W. Plank, M. Hulman, C. Kramberger, A. Grüneis, T. Pichler, H. Peterlik, H. Kataura, and Y. Achiba, Eur. Phys. J. B **22**, 307 (2001).
[21] G. Kresse and D. Joubert, Phys. Rev. B **59**, 1758 (1999).
[22] V. Zólyomi, J. Koltai, J. Kürti, and H. Kuzmany, in *DFT Calculations on Fullerenes and Carbon Nanotubes*, edited by V. A. Basiuk and S. Irle (Research Signpost, India, 2008), p. 297.
[23] S. Reich, C. Thomsen, and J. Maultzsch, *Carbon Nanotubes* (Wiley-VCH, Weinheim, 2004).
[24] Slightly different values are given in Ref. 19 when the Raman dispersion was studied for visible laser excitations only.
[25] S. Piscanec, M. Lazzeri, J. Robertson, A. C. Ferrari, and F. Mauri, Phys. Rev. B **75**, 035427 (2007).
[26] C. Fantini, A. Jorio, M. Souza, M. S. Strano, M. S. Dresselhaus, and M. A. Pimenta, Phys. Rev. Lett. **93**, 147406 (2004).
[27] H. Telg, J. Maultzsch, S. Reich, F. Hennrich, and C. Thomsen, Phys. Rev. Lett. **93**, 177401 (2004).
[28] Cutting lines denote the k points allowed for SWCNTs in the graphene Brillouin zone.
[29] S. M. Bachilo, M. S. Strano, C. Kittrell, R. H. Hauge, R. E. Smalley, and R. B. Weisman, Science **298**, 2361 (2002).
[30] V. N. Popov and L. Henrard, Phys. Rev. B **70**, 115407 (2004).
[31] V. Zólyomi and J. Kürti, Phys. Rev. B **70**, 085403 (2004).
[32] X. Blase, L. X. Benedict, E. L. Shirley, and S. G. Louie, Phys. Rev. Lett. **72**, 1878 (1994).